Int. J. Heat Mass Transfer. Vol. 10, pp. 499–518. Pergamon Press Ltd. 1967. Printed in Great Britain

CALCULATION OF HEAT TRANSFER TO TURBINE BLADING IN THE PRESENCE OF SECONDARY FLOW

L. A. WALKER and E. MARKLAND
The Universities of Leeds and Belfast

(*Received* 7 *July and in revised form* 13 *October* 1966)

Abstract—A previous paper [1] has described measurements of local heat-transfer coefficients over the surface of a gas turbine blade in a cascade where strong secondary flow was generated. Details of calculations are now given, the work being considered in two parts: (a) the estimation of secondary flow velocities and (b) the nature of the blade boundary layer and related heat-transfer properties.

In the first part, calculations for the induced streamwise vorticity are based on the method of Hawthorne [2]. The calculations are made with three assumptions, of various degrees of refinement, about the main flow. In the simplest case a free vortex flow is assumed, in the next a known two-dimensional velocity field about the blades is used, and finally, this is corrected to allow for displacement of the main stream. The results do not differ greatly from each other, and agreement with experiment is generally good.

Boundary-layer calculations make use of the momentum integral relations in the form due to Mager [3] for three-dimensional flow. Adaptations are made to allow for mainstream vorticity where this is significant, and to incorporate a more general skin friction law.

Heat transfer in the laminar layer is calculated by Squire's method [4] and for the turbulent boundary layer by using Von Kármán's extension of Reynolds analogy. The difficulty of predicting conditions following a laminar separation has made it necessary to base the initial data for a reattaching turbulent layer on an empirical rule, which is tentatively suggested for wider application, obtained from measured heat-transfer data.

Comparison with experiment is good where the boundary-layer is laminar, but the heat transfer is overestimated in turbulent regions, particularly in the presence of a favourable pressure gradient.

NOMENCLATURE

a, n, coefficients in empirical fit to Prandtl–Schlichting friction law;
c, blade chord;
C, $= \partial\beta/\partial x = 1/\sigma$ curvature of streamline;
d, diameter of cylinder descriptive of the leading edge of the blades;
f_1, $= \partial U/\partial x$ streamwise gradient of primary velocity;
$\bar{F}$, body force vector,
g, G, functions defining velocity profiles in the blade boundary layer;
h, local heat-transfer coefficient;
k, thermal conductivity;
H, J, K, L, boundary layer shape factors defined by equations (4.9);
m, $= P_{xz}/P_{2c}$ ratio of total pressure at chosen point of blade passage to total pressure on centre line;
Nu, Nusselt number hc/k; $Nu_d = hd/k$, $Nu_x = hx/k$;
p, P, local static, total pressure;
Pr, Prandtl number;
R, radius measured from axis of rotation of blade;
Re, Reynolds number; $Re_2 = U_{2c}c/\nu$, $Re_d = U_{1z}d/\nu$; $Re_\theta = U_x\theta_x/\nu$, $Re_x = U_x x/\nu$;
S, distance measured along streamline;
u, v, w, components of secondary velocity in x, y, z directions;
U, scalar magnitude of $\bar{V}$;
$\bar{V}$, velocity vector;
x, y, z, co-ordinate directions referred to two-dimensional potential flow pattern, defined in Fig. 1;

$\mathbf{x}, \mathbf{y}, \mathbf{z}$, co-ordinate directions used in development of boundary-layer equations;

Z, local skin friction parameter defined by $Z^2 = \rho u_x^2/\tau_{0.x}$.

Greek symbols

α, $= \tan^{-1} \tau_{0,z}/\tau_{0,x}$ angle between surface stress and direction of U outside boundary layer;

β, angle between stream direction and (xy) plane;

δ, boundary-layer thickness;

δ_T, thermal boundary-layer thickness;

δ_x^*, δ_z^*, displacement thickness of boundary layer defined in equations (4.5);

ε $= \tan \alpha$;

θ, angular deflection of streamline in (xy) plane;

$\theta_x, \theta_{xz}, \theta_z$, momentum thicknesses of boundary-layer defined in equations (4.5);

$\boldsymbol{\theta}$, $= \theta_x Re_\theta^n$;

$\boldsymbol{\theta}_{\mathrm{I}}, \boldsymbol{\theta}_{\mathrm{II}}$, first and second approximations to $\boldsymbol{\theta}$;

Λ, $= \dfrac{\delta^2}{\nu} \dfrac{\mathrm{d}u}{\mathrm{d}x}$ velocity gradient parameter;

μ, ν, ρ, dynamic, kinematic viscosity, density of fluid;

ξ, η, ζ, components of $\overline{\Omega}$ in x, y, z directions;

σ, radius of curvature of streamline;

τ, shear stress;

τ_{xy}, τ_{zy}, shear stress in (**xy**) and (**zy**) planes;

$\tau_{0.x}$, surface shear stress in direction of **x**;

$\tau_{0.z}$, surface shear stress in direction of **z**;

ϕ, angle between normals to streamline and Bernoulli surface;

ψ, secondary stream function;

$\overline{\Omega}$, vorticity vector;

ω, scalar magnitude of blade angular velocity about a fixed axis;

$\omega_x, \omega_y, \omega_z$, components of blade angular velocity in **x**, **y**, **z** directions.

Suffixes

1, upstream condition;

1z, upstream condition at distance z from midspan;

2, downstream condition;

2c, downstream condition at midspan;

x, condition at distance x measured along streamline;

xz, condition at point in blade passage at distance z from midspan.

1. THE SECONDARY STREAM

THE SECONDARY stream is calculated by use of Hawthorne's theory [2] which is indicated briefly below. It has been used by Hawthorne and Armstrong [5] to predict with fair accuracy the secondary flow at outlet from a cascade of impulse turbine blades; moreover, other theories of Squire and Winter [6] and Preston [7] are seen to be special cases of the theory.

The equations refer to inviscid incompressible flow. The vorticity present upstream of the deflecting cascade may have arisen from frictional effects, but in the deflecting mainstream with which we are concerned, viscous effects are not influential in forming the secondary flow.

With $\overline{V}$ as a stream velocity vector of scalar magnitude U, the vorticity $\overline{\Omega} = \text{curl } \overline{V}$ may be split into two components

$$\left(\frac{\overline{\Omega} \cdot \overline{V}}{\overline{V} \cdot \overline{V}}\right) \overline{V} = \left(\frac{\xi}{U}\right) \overline{V} \quad \text{directed along the streamline}$$

and

$$\frac{(\overline{V} \wedge \overline{\Omega}) \wedge \overline{V}}{\overline{V} \cdot \overline{V}} \quad \text{normal to the streamline.}$$

The following relations are used:

$$\text{div } \overline{\Omega} = 0, \text{ since } \overline{\Omega} = \text{curl } \overline{V}$$

$$\text{div } \overline{V} = 0 \text{ by continuity.}$$

The analysis considers the estimation of the streamwise component of vorticity. The foregoing relations may be used to show that

$$\bar{V} \cdot \text{grad}\left(\frac{\xi}{U}\right) = \frac{\text{div}\,\bar{V} \wedge (\bar{V} \wedge \bar{\Omega})}{U^2} \quad (1.1)$$

of which the right-hand side is expanded using the Euler equation

$$(\bar{V} \cdot \text{grad})\,\bar{V} = -\text{grad}\left(\frac{p}{\rho}\right) + \bar{F}$$

where $\bar{F}$ represents body forces. The resulting expression derived in [2] is

$$\bar{V} \cdot \text{grad}\left(\frac{\xi}{U}\right) = -\frac{1}{U^4}\left\{\left[2\bar{V} \wedge \text{grad}\left(\frac{P}{\rho}\right)\right] \cdot (\bar{V} \cdot \text{grad})\,\bar{V}\right\} - \frac{1}{U^2}(\bar{F} \cdot \bar{\Omega}) - \text{div}\,\frac{(\bar{V} \wedge \bar{F})}{U^2}. \quad (1.2)$$

The first term on the right-hand side is shown to arise as the forward inclination in the stream direction of an upstream vortex line in transit through the passageway. The second term, which becomes effective downstream, represents the wake-directed component arising from stretching of a portion of the filament that commences upstream and wraps round the blade in passage. The third is the vorticity shed from the blade due to change of circulation along its length in non-uniform flow.

Within the blade space, only the first right-hand term of equation (1.2) is retained. Examining this term, the argument of Hawthorne [8] shows that only the centripetal component U^2/σ (in which σ is the radius of curvature of the streamline) of acceleration $(\bar{V} \cdot \text{grad})\,\bar{V}$ contributes to the result of the scalar product. In general, the Bernoulli surfaces are curved as well as the streamlines, and the normal to the Bernoulli surface at any point is not perpendicular to the principal normal to the streamline. Writing ϕ as the angle between these normals, equation (1.2) becomes

$$\bar{V} \cdot \text{grad}\left(\frac{\xi}{U}\right) = -2\frac{U}{U^4}\left\{\text{grad}\left(\frac{P}{\rho}\right)\right\}\frac{U^2}{\sigma}\sin\phi.$$

Integrating this expression between stations 1 and 2 of a streamline along which the length is denoted by S, leads to the result

$$\left(\frac{\xi}{U}\right)_2 - \left(\frac{\xi}{U}\right)_1 = -2\int_1^2 \frac{1}{U^2}\left\{\text{grad}\left(\frac{P}{\rho}\right)\right\}\frac{\sin\vartheta}{\sigma} \cdot \text{d}S.$$

In the present case, Bernoulli surfaces are assumed to be plane and parallel to the end wall so that $\phi = \pi/2$. Replacing $\text{d}S/\sigma$ in this by the streamline deflection $\text{d}\theta$ and performing the integration from the upstream direction where $\xi = 0$,

$$(\xi/U) = -2\int_1 \frac{1}{U^2}\,\text{grad}\,(P/\rho)\,\text{d}\theta. \quad (1.3)$$

If U is constant along any given streamline (as in free vortex flow) and if grad (P/ρ) is assumed to be constant along the streamline, i.e.

$$\text{grad}\,(P/\rho) = \text{grad}\,(p_1/\rho + U_1^2/2) = U_1(\text{d}U_1/\text{d}z)$$

then equation (1.3) becomes

$$\xi = -2(\text{d}U_1/\text{d}z)\,\theta \quad (1.4)$$

which is the result of Squire and Winter [6].

2. EVALUATION OF THE STREAMWISE-DIRECTED VORTICITY

Figure 1 indicates the position of (yz) planes, a', etc., in which the vorticity component ξ and the resulting induced velocities v, w are to be computed. The planes do not quite coincide with the slightly curved equipotential planes of two-dimensional motion, but no significant error is introduced by this discrepancy. ξ is

computed from the integral of equation (1.3) in the form

$$\left(\frac{\xi}{U}\right)_{xz} = -2\int_1^x \frac{1}{U_{xz}^2} \text{ grad } (P_{xz}/\rho)/\mathrm{d}\theta \quad (2.1)$$

where the suffix xz is introduced to identify a chosen point in the blade passage at a specified spanwise station z. The terms $U_{xz}P_{xz}$ and θ of the integrand define the "primary field" in the sense used in [1], and, irrespective of the degree of sophistication adopted in describing this field, it should be noted that perturbations introduced by the secondary velocities are neglected when evaluating the integral. The main features of the primary field are recalled at the end of this section.

Equation (2.1) is conveniently written for the purpose of calculation as

$$\xi_{xz} = -\frac{2}{U_{1z}}\left(\frac{U_{xz}}{U_{1z}}\right)\frac{P_{2c}}{\rho}\int_1^x \frac{\partial m}{\partial z}\left(\frac{U_{1z}}{U_{xz}}\right)^2 \mathrm{d}\theta \quad (2.2)$$

in which P_{2c} is a convenient reference pressure (the total pressure downstream at the centre span), U_{1z} is the upstream velocity in the (xy) plane under consideration, and m is P_{xz}/P_{2c}. The integral may be evaluated along the streamlines of Fig. 1 for a specified distribution of upstream total pressure, on the assumptions that $\partial m/\partial z$ remains constant, and U_{1z}/U_{xz} retains the value it has in two-dimensional flow, as the integration proceeds. Alternatively, the measured field within the blade passages may be used to derive appropriate values for the total pressure gradient and velocity along the length of the streamline to perform a more realistic calculation, so obtaining a comparison of computations of two different degrees of refinement. The details are given in Appendix 1; it suffices to note here that in the region where the upstream total pressure is uniform a different expression is used from that appropriate to the region where there are severe gradients of total pressure.

The calculation of vorticity according to equation (1.4) due to Squire and Winter [6] follows immediately from

$$\xi = -2(\mathrm{d}U_1/\mathrm{d}z)\,\theta = -2\theta\,\mathrm{d}[2(P_{1z} - p_1)/\rho]/\mathrm{d}z \quad (2.3)$$

in which θ is angular deflection as read from the two-dimensional flow pattern of Fig. 1 and P_{1z} is assumed constant along a streamline, being specified in terms of z upstream of the cascade.

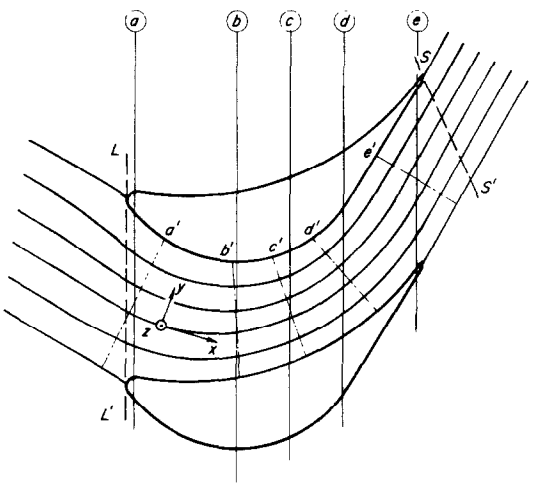

FIG. 1. Two-dimensional potential flow solution and planes used for measurement and for calculation of secondary velocities.

Note on the primary velocity field

Certain main features of the primary velocity field referred to above have been described in reference [1], where it was seen that results of the potential solution disagreed slightly with measured pressure data at the blade surfaces even over the portion of the blade span where total pressure is uniform, and that there was a small decrease in static pressure drop across the cascade as compared with the two-dimensional value, due to the reduction in stream exit angle caused by secondary velocities. This particular influence outweighed a reverse effect due to a net contraction of the width of the stream over

which the total pressure is uniform, which tends to promote an increased pressure drop across the cascade. In passing through the blading, the mainstream is deflected laterally with the changing velocity profile. An accurate prediction of this, as a basis for evaluating the terms of the integrand of the equation for streamwise component of vorticity would be complex but might be made in terms of the actuator disc theory as developed by Hawthorne and Armstrong [9], where the equations of continuity and motion are linearized on replacing the cascade by a disc at which deflection occurs. Application of the equations is limited to fields of moderate upstream non-uniformity, so it is not surprising that when a prediction was made in this way for the total pressure profile at the plane of trailing edges, the result did not tally with experiment in respect of the dimensions of the uniform region.

Rather than attempting to extend the method of Hawthorne and Armstrong [9], recourse was made to experimental data to obtain a more refined primary field. Whilst such information may not in general be available for cascades of blades, it is useful to determine to what extent the computed secondary velocities are affected by the assumptions made concerning the primary field. In fact it will be seen that secondary velocities based on the relatively simple potential field, which makes no appeal to experimental measurements within the blade passage, and corrected simply in terms of an upstream velocity profile, compare favourably with those based on the lengthier method. Even assuming a free vortex field, which leads to Squire and Winter's result of equation (2.3), gives results of fair accuracy.

3. SOLUTION FOR THE INDUCED VELOCITIES v AND w

The vorticity component ξ has the direction of the unperturbed streamline, so that induced velocities lie in the equipotential surfaces which are normal to the streamlines. These surfaces are very nearly plane so the plane surfaces indicated by a', etc., in Fig. 1 may be regarded as equipotentials for present purposes, and the components v and w may be evaluated as if directions y and z lay in these plane surfaces.

The local vorticity and continuity relations are

$$\xi = \frac{\partial w}{\partial y} - \frac{\partial v}{\partial z} \tag{3.1}$$

$$\frac{\partial}{\partial x}(U \cos \beta + u) + \frac{\partial y}{\partial y} + \frac{\partial w}{\partial z} = 0 \tag{3.2}$$

where u, v, and w are perturbation components, U is the mainstream primary velocity and β is the angle between the mainstream direction and the (xy) plane. The perturbation value u is taken as being small compared with v and w since it arises only from reorientation of the incident vorticity η_1, out of the (xy) plane, giving a component ζ, under the action of the secondary components v and w, and is therefore of a smaller order of magnitude.

The distribution of β over the blade is as yet unknown, so the assumption is made that cos $\beta = 1$. Values of w resulting from a calculation using this assumption could, if required, be used to obtain a better approximation to cos β. The results of Figs. 6 and 7, for the particular calculation reported here, show that the assumption is reasonably valid up to $x/c \simeq 0{\cdot}9$ on the convex surface and up to $x/c \simeq 0{\cdot}6$ on the concave. Writing the known variation of $\partial U/\partial x$ in the (yz) plane as $f_1(y, z)$, and taking cos $\beta = 1$, equation (3.2) becomes

$$f_1(y, z) + \partial v/\partial y + \partial w/\partial z = 0. \tag{3.3}$$

Appropriate differentiation of equations (3.1) and (3.3) gives

$$\frac{\partial^2 v}{\partial y^2} + \frac{\partial^2 v}{\partial z^2} = -\frac{\partial f_1}{\partial y} - \frac{\partial \xi}{\partial z} \tag{3.4}$$

$$\frac{\partial^2 w}{\partial y^2} + \frac{\partial^2 w}{\partial z^2} = -\frac{\partial f_1}{\partial z} + \frac{\partial \xi}{\partial y}. \tag{3.5}$$

The right-hand terms of equations (3.4) and (3.5) are not easily described by analytical functions nor are the values of v and w initially

known round the entire boundary of the cross-section of the flow passage.

An initial approximation, however, may be made taking the assumption $f_1 = 0$. This allows the definition of a secondary stream function according to

$$v = \frac{\partial \psi}{\partial z}; \qquad w = -\frac{\partial \psi}{\partial y} \tag{3.6}$$

which satisfies the reduced equation

$$\frac{\partial v}{\partial y} + \frac{\partial w}{\partial z} = 0. \tag{3.2a}$$

Rewriting the relation (3.1) gives

$$\frac{\partial^2 \psi}{\partial y^2} + \frac{\partial^2 \psi}{\partial z^2} = -\xi \tag{3.7}$$

where $\psi = 0$ round the entire boundary of the flow passage, and along the plane of symmetry $z = 0$.

A relaxation solution for ψ is found for each of the planes a' to e' of Fig. 1, the distribution of ξ over each of the planes being determined by one of the methods described in Section 2. A similar procedure may now be followed for evaluation of $\partial U/\partial x$ where U originates in the potential solution, and is taken to vary in the direction of z in direct proportion to the upstream velocity. Boundary values are then given to equations (3.4), (3.5) which, by the relaxation method, yield an improved solution for v and w.

It will be seen that with the assumption $\partial U/\partial x = 0$ (which is true only for flow approaching and receding from the cascade), equations (3.4) and (3.5) become

$$\frac{\partial^2 v}{\partial y^2} + \frac{\partial^2 v}{\partial z^2} = -\frac{\partial \xi}{\partial z} \tag{3.4a}$$

$$\frac{\partial^2 w}{\partial y^2} + \frac{\partial^2 w}{\partial z^2} = +\frac{\partial \xi}{\partial y}. \tag{3.5a}$$

Results computed for v and w on these relations must be identical with those derived from the stream function via equations (3.6) and (3.7), apart perhaps from some loss of accuracy in the use of the differentiated right hand quantities in the above pair of equations. The order of differences to be expected between the solution based on equations (3.4) and (3.5) and the first approximation based on equation (3.7) will be indicated by the respective magnitudes of $-\partial f_1/\partial y$ compared with $-\partial \xi/\partial z$ in equation (3.4) and $-\partial f_1/\partial z$ compared with $+\partial \xi/\partial y$ in equation (3.5).

Figures 2 and 3 show the results of calculations in which the streamwise component of vorticity ξ has been calculated by the three different methods referred to above, and the resulting induced velocities by equation (3.7). Correspondence with experiment is generally quite good, but it cannot be argued that increasingly good agreement results from increasingly complicated calculation.

Plane e was selected to illustrate the secondary velocity distributions, partly to amplify the data given in reference [1] where similar results were given for plane c, and partly because secondary velocities generally have their largest values at plane e.

The effect of including the f_1 term is illustrated on Figs. 4 and 5, where a comparison is made, using the same distribution of ξ in both cases, between the secondary velocities computed by equation (3.7) and by solution of equations (3.4) and (3.5). The w component is altered very little by inclusion of f_1, but v is affected to a noticeable amount and generally agrees rather better with measurements than the previous solution. It should be noted that calculations done in plane e' have been corrected to plane e, by increasing v and w in proportion to the increase of the deflection angle in two-dimensional flow from plane e' to plane e.

4. THE THREE-DIMENSIONAL BOUNDARY LAYER AND HEAT-TRANSFER PREDICTIONS

The mechanism which produces secondary flow in the turning mainstream is also present in the blade boundary layer, where severe total pressure gradients are present, and where more pronounced spanwise deflections are to be

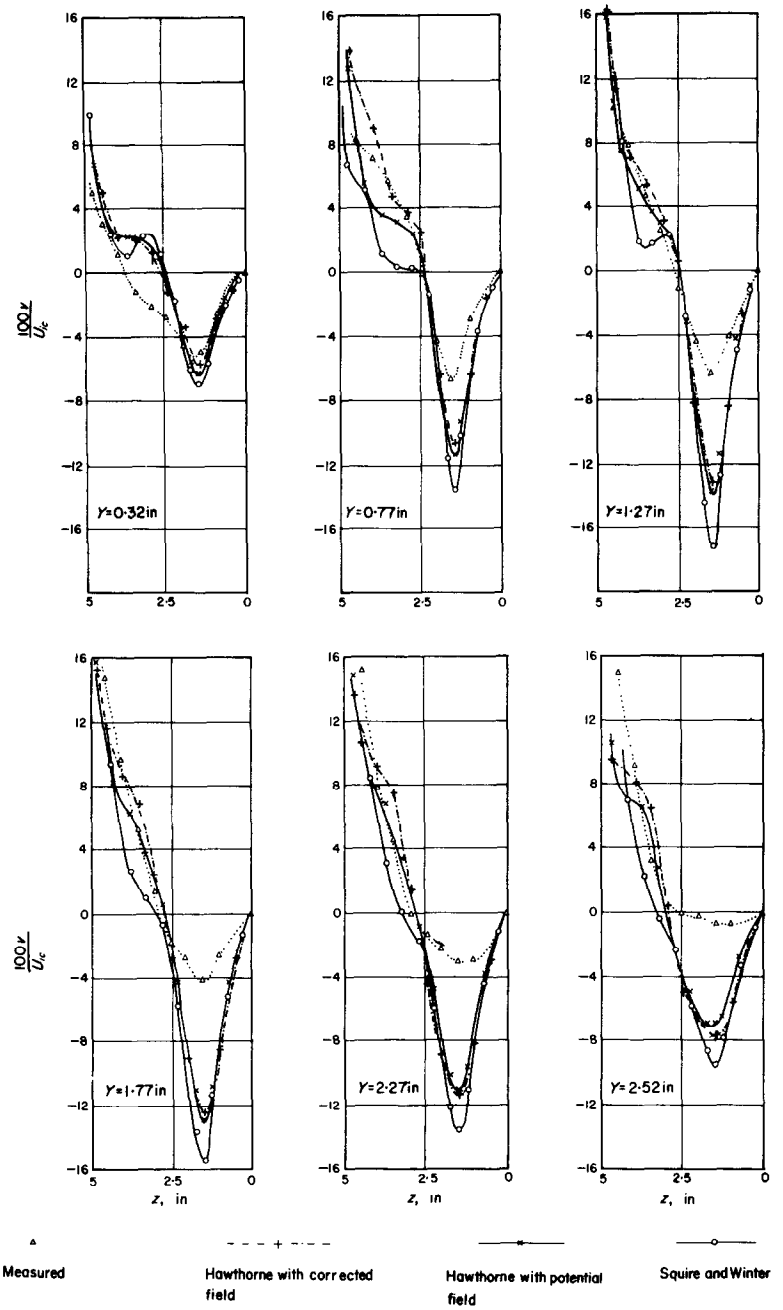

FIG. 2. Component of secondary flow in y-direction at plane e—streamwise velocity gradient neglected. Y measured in direction of cascade from mid point of LL' of Fig. 1, z measured in direction of span from mid point of blade.

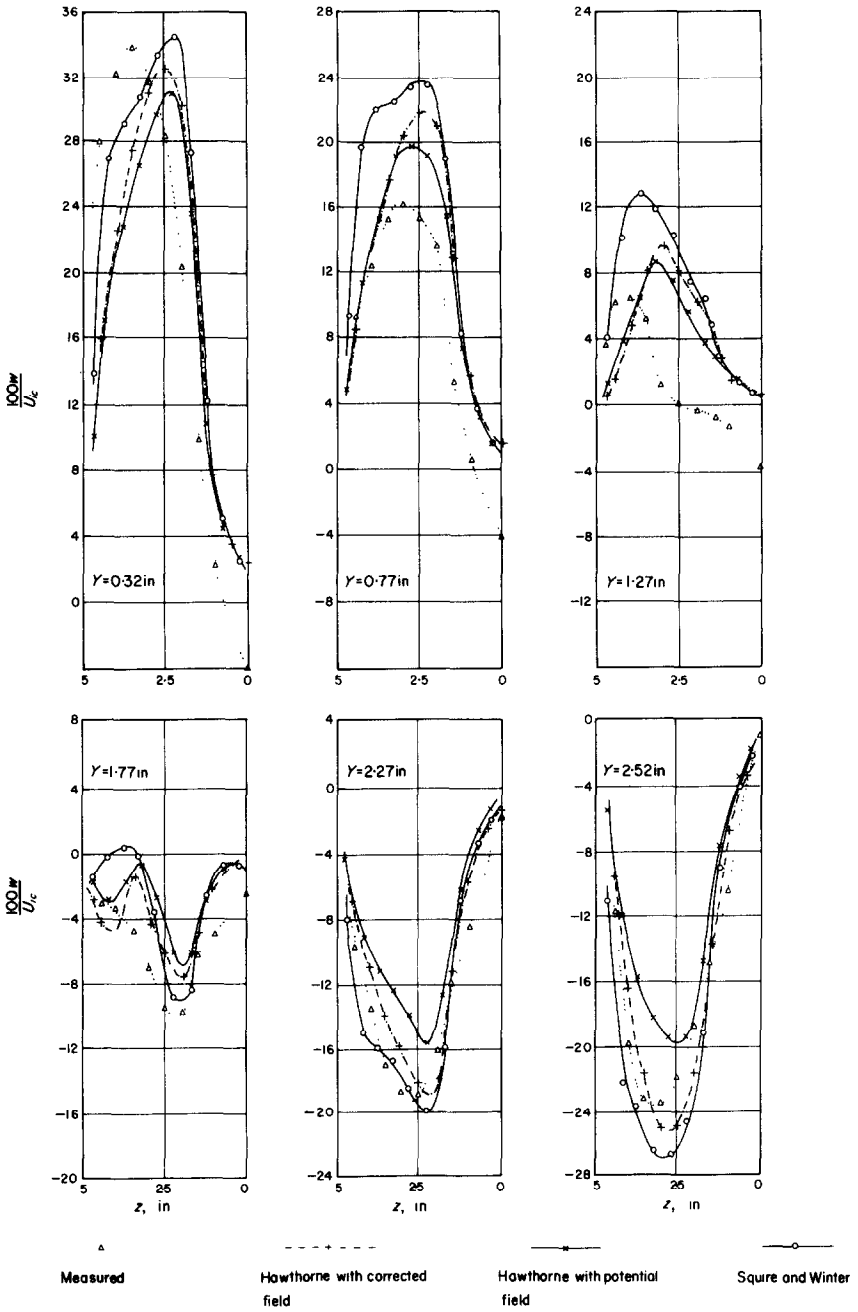

FIG. 3. Component of secondary flow in z-direction at plane e—streamwise velocity gradient neglected. Y measured in direction of cascade from mid point of LL' of Fig. 1, z measured in direction of span from mid point of blade.

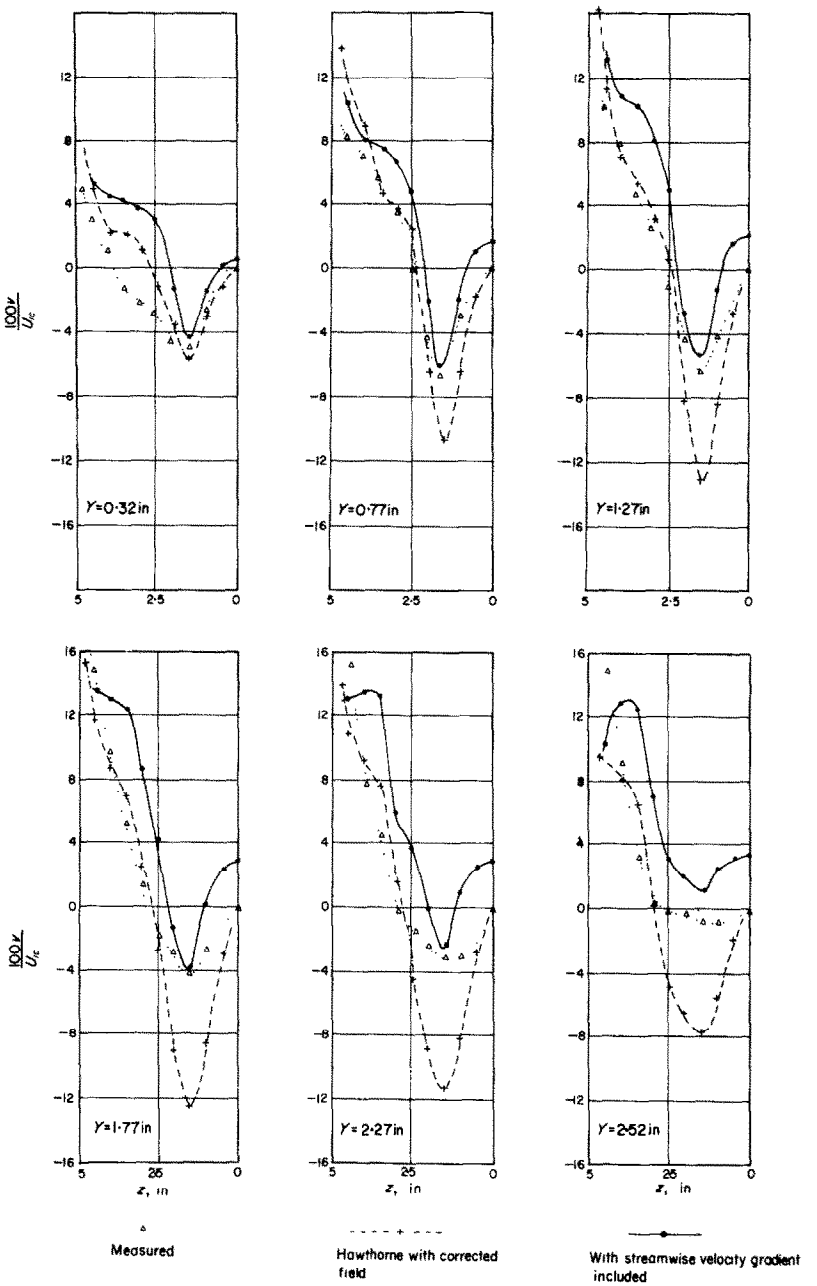

FIG. 4. Effect of including streamwise velocity gradient on component of secondary flow in y-direction. Y measured in direction of cascade from mid point of LL' of Fig. 1, z measured in direction of span from mid point of blade.

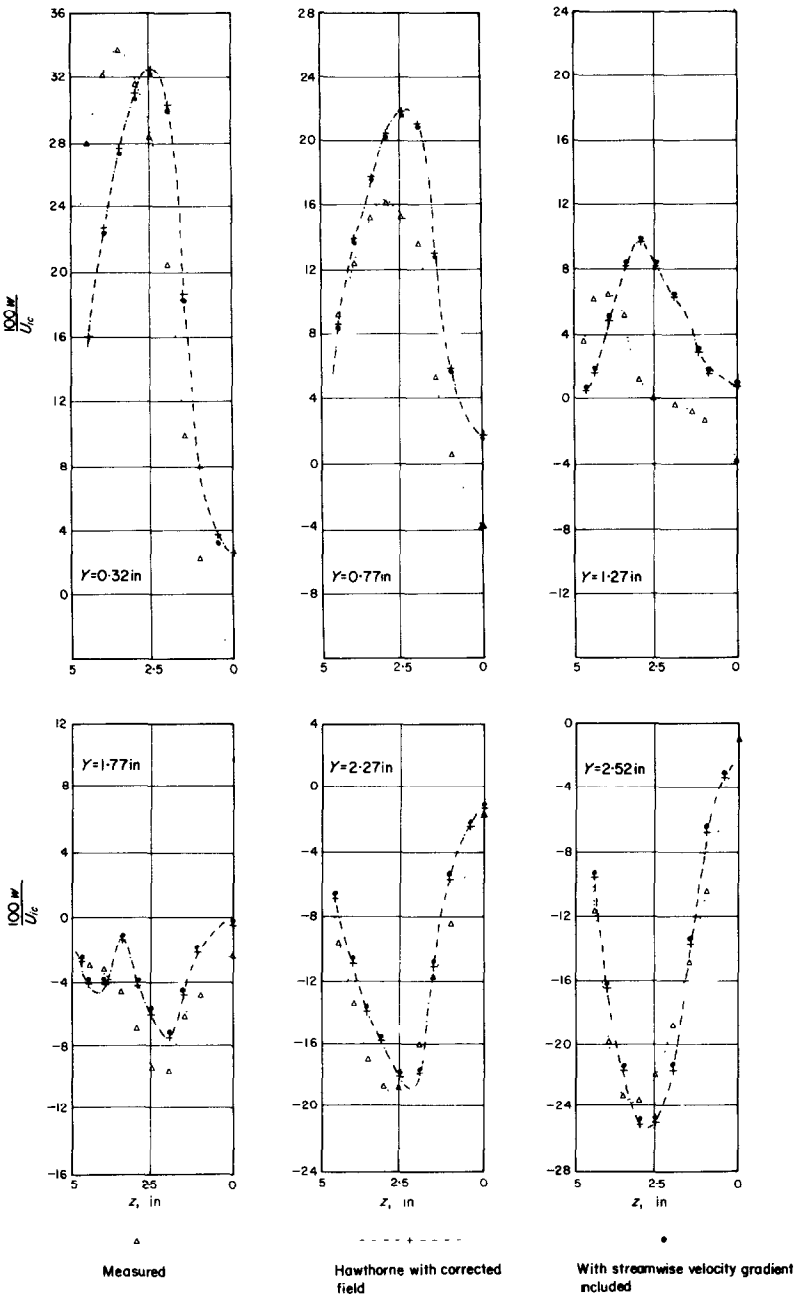

FIG. 5. Effect of including streamwise velocity on component of secondary flow in z-direction. Y measured in direction of cascade from mid point of LL' of Fig. 1, z measured in direction of span from mid point of blade.

expected near to the surface. It is therefore convenient to divide the velocity in the boundary layer into two components at right angles, the axes being chosen either with reference to the (xy) plane of Fig. 1 or with reference to the velocity vector just outside the boundary layer.

The problem has been treated by Wild [10], Timman [11], Mager [3] and others. Timman provides the most general method, allowing the main and cross flow components to vary arbitrarily in relation to a curved surface. However, with the one restriction that the cross flow varies with respect to the streamwise coordinate only, the method due to Mager [3] appears to be applicable to this problem and was adopted with some modification.

Mager shows that the boundary-layer equations referred to the orthogonal curvilinear co-ordinate system (**x**, **y**, **z**), rotating with uniform angular velocity ω, and in which **x** is the stream direction just outside the boundary layer and **y** is normal to the surface, may be written as

$$u\frac{\partial u}{\partial \mathbf{x}} + v\frac{\partial u}{\partial \mathbf{y}} + w\frac{\partial u}{\partial \mathbf{z}} + Cuw = -\frac{1}{\rho}\frac{\partial p}{\partial \mathbf{x}} + \frac{1}{\rho}\frac{\partial \tau_{xy}}{\partial \mathbf{y}} + \omega^2 R\frac{\partial R}{\partial \mathbf{x}} - 2\omega_y w \quad (4.1)$$

$$u\frac{\partial w}{\partial \mathbf{x}} + v\frac{\partial w}{\partial \mathbf{y}} + w\frac{\partial w}{\partial \mathbf{z}} - u^2 C = -\frac{1}{\rho}\frac{\partial p}{\partial \mathbf{z}} + \frac{1}{\rho}\frac{\partial \tau_{zy}}{\partial \mathbf{y}} + \omega^2 R\frac{\partial R}{\partial \mathbf{z}} + 2\omega_y u. \quad (4.2)$$

In these equations, (u, v, w) are velocity components within the boundary layer and C is the curvature of the **x**-axis. For a laminar boundary layer, $\partial\tau_{xy}/\partial\mathbf{y}$ may be replaced by $\mu(\partial^2 u/\partial\mathbf{y}^2)$ and $\partial\tau_{zy}/\partial\mathbf{y}$ by $\mu(\partial^2 w/\partial\mathbf{y}^2)$. Adapting Mager's treatment to the present case where there is a component η of vorticity in the **y** direction just outside the boundary layer and where ω is zero, the momentum equations may be shown to be

$$\frac{\partial\theta_x}{\partial \mathbf{x}} + \frac{1}{U}\frac{\partial U}{\partial \mathbf{x}}(2\theta_x + \delta_x^*) + \frac{\partial\theta_{xz}}{\partial \mathbf{z}} + \frac{2\eta}{U}\theta_{xz} = \frac{\tau_{0.x}}{\rho U^2} \quad (4.3)$$

$$\frac{\partial\theta_z}{\partial \mathbf{z}} + \frac{\partial}{\partial \mathbf{x}}(\delta_z^* - \theta_{xz}) + \frac{1}{U}\frac{\partial U}{\partial \mathbf{z}}(\theta_z - \theta_x - \delta_x^*) + \frac{2}{U}\frac{\partial U}{\partial \mathbf{x}}(\delta_z^* - \theta_{xz}) + \frac{\eta}{U}(\theta_x + \theta_z) = -\frac{\tau_{0.z}}{\rho U^2} \quad (4.4)$$

where U is the value of u at the edge of the boundary layer, $\tau_{0.x}$ and $\tau_{0.z}$ are surface shear stress components in the **x**- and **z**-directions, and displacement and momentum thicknesses are defined as follows:

$$\left.\begin{aligned} \theta_x &= 1/U^2 \int (U-u)u\,\mathrm{d}\mathbf{y} \\ \theta_{xz} &= 1/U^2 \int (U-u)w\,\mathrm{d}\mathbf{y} \\ \theta_z &= 1/U^2 \int w^2\,\mathrm{d}\mathbf{y} \\ \delta_x^* &= 1/U \int (U-u)\,\mathrm{d}\mathbf{y} \\ \delta_z^* &= 1/U \int w\,\mathrm{d}\mathbf{y}. \end{aligned}\right\} \quad (4.5)$$

To obtain a solution of the momentum equations it is necessary to assume expressions for u and w; Mager followed Prandtl's suggestion [12]

$$\left.\begin{aligned} u/U &= G(\mathbf{y}/\delta) \\ w/U &= \varepsilon G(\mathbf{y}/\delta)\, g(\mathbf{y}/\delta) \end{aligned}\right\} \quad (4.6)$$

in which G and g are functions undefined at present, satisfying the following boundary conditions,

$$\begin{aligned} \text{when}\quad \mathbf{y} = 0: &\quad G = 0, \quad g = 1 \\ \mathbf{y} = \delta: &\quad G = 1, \quad g = 0 \end{aligned} \quad (4.7)$$

and in which ε is

$$\varepsilon = \tan\alpha = \tau_{0.z}/\tau_{0.x} \quad (4.8)$$

α being the angle between the surface stress and the direction of U.

It is convenient to introduce constants

defined by Mager in terms of the functions G and g as follows

$$\left.\begin{aligned} H &= \int(1-G)\,\mathrm{d}y/\int(1-G)G\,\mathrm{d}y \\ J &= \int(1-G)Gg\,\mathrm{d}y/\int(1-G)G\,\mathrm{d}y \\ K &= \int Gg\,\mathrm{d}y/\int(1-G)G\,\mathrm{d}y \\ L &= \int G^2g^2\,\mathrm{d}y/\int(1-G)G\,\mathrm{d}y \end{aligned}\right\} \quad (4.9)$$

so that the various boundary-layer thicknesses may be written in terms of θ_x as

$$\delta_x^* = H\theta_x, \qquad \theta_{xz} = \varepsilon J\theta_x, \qquad \delta_z^* = \varepsilon K\theta_x, \qquad \theta_z = \varepsilon^2 L\theta_x. \quad (4.10)$$

For calculation of the laminar boundary layer of the turbine blade profile, the function $G(y/\delta)$ is assumed to be of the Pohlhausen quartic form

$$G(y/\delta) = (2 + \Lambda/6)(y/\delta) - (\Lambda/2)(y/\delta)^2 + (-2 + \Lambda/2)(y/\delta)^3 + (1 - \Lambda/6)(y/\delta)^4 \quad (4.11)$$

in which

$$\Lambda = \frac{\delta^2}{\nu}\frac{\mathrm{d}U}{\mathrm{d}x} \quad (4.12)$$

The function $g(y/\delta)$ is taken as

$$g(y/\delta) = (1 - y/\delta)^2 \quad (4.13)$$

which is the form successfully used by Mager for turbulent layers when computing results for comparison with experimental data of Gruschwitz [13]. Its use for laminar layers has been proposed by Prandtl [12] for a yawed cylinder. The Pohlhausen profile is known to give good accuracy for laminar boundary layers which are not close to separation, and reasonable confidence is put in equation (4.11) provided that the velocity gradient parameter Λ can be suitable chosen. After some analysis of the results of Squire [4], a value of $\Lambda = 3{\cdot}0$ was assumed for the laminar boundary layer on both of the blade surfaces. The corresponding constants required for subsequent calculations are

$H = 2{\cdot}430$, $J = 0{\cdot}492$, $K = 1{\cdot}365$ and $L = 0{\cdot}2445$.

However, for evaluation of the momentum thickness θ, equation (4.17) below, due to Squire, was adopted.

The turbulent layer solution requires assumptions regarding surface shear stress as well as velocity profiles. Following Mager, we adopt

$$G = (y/\delta)^{\frac{1}{4}}, \qquad g = (1 - y/\delta)^2 \quad (4.14)$$

which leads to

$$H = 1{\cdot}2857, \qquad J = 0{\cdot}5423, \qquad K = 2{\cdot}6727, \qquad L = 1{\cdot}0285.$$

However, the friction law which he used is replaced by a somewhat more general form

$$\tau_{0.x}/\rho U_x^2 = \alpha(Re_\theta)^{-n}. \quad (4.15)$$

Values of a and n are chosen so that the resulting value of $\tau_{0.x}$, computed at a value of Re_θ corresponding to the start of the turbulent layer and at ten times this value, agree with the Prandtl–Schlichting values at the same pair of values of Re_θ. The integration of equations (4.3) and (4.4) is then possible as indicated in Appendix 2. For the purpose of subsequent heat-transfer calculations, the required momentum thickness is θ_x, and this is conveniently rewritten at this stage as

$$\theta = \theta_x\, Re_\theta^n. \quad (4.16)$$

Appendix 2 gives details of the method by which the momentum integral equations may be solved. Successive approximations for θ, designated by θ_{I} and θ_{II}, are obtained for the momentum thickness under two- and three-dimensional conditions respectively.

Heat-transfer calculation

As a preliminary to calculating heat-transfer coefficients the momentum thickness is determined over the surface under conditions of cross-flow by the methods referred to above.

For the laminar layer, the appropriate values of a and n are 0·235 and 1·0 respectively, corresponding to the adoption of Pohlhausen's velocity profile. However, the form used by Squire [4] is known to be reliable for laminar boundary-

layer calculation, so the value of θ_x is taken to be given by

$$\theta_x^2 = \frac{0{\cdot}441\,\nu}{U_x^6}\int_0^x U^5\,\mathrm{d}x. \qquad (4.17)$$

The numerical values of the shape factors H, J, K and L are taken to be constant throughout, since they do not vary greatly.

The well-known result of Squire's calculation is

$$h = 0{\cdot}5715\,k/\delta_T \qquad (4.18)$$

where δ_T is the thermal boundary-layer thickness which may be obtained iteratively from the physical thickness using tabulated functions and the known variation of U in the stream. For the purpose of comparison with experiment, it is convenient to express this in the form

$$\frac{Nu}{Re_2^{\frac{1}{2}}} = \frac{0{\cdot}5715}{(\delta_T/c)\,Re_2^{\frac{1}{2}}} \qquad (4.19)$$

in which Nu is the Nusselt number based on blade chord c and Re_2 is Reynolds number referred to downstream conditions at midspan of the blades. For the stagnation point, the empirical relation given by Squire, which closely fits his exact solution, is used:

$$\frac{Nu_d}{Re_d^{\frac{1}{2}}} = 1{\cdot}14\,Pr^{0{\cdot}4} \qquad (4.20)$$

in which d is the cylinder diameter descriptive of the leading edge. Expressed in the same form as equation (4.19)

$$\frac{Nu}{Re_2^{\frac{1}{2}}} = 1{\cdot}14(cU_{1z}/dU_{2c})^{\frac{1}{2}}\,Pr^{0{\cdot}4} \qquad (4.21)$$

No attempt has been made so far to allow for the influence of nose vortices mentioned in the discussion of experiments in the first paper, although this may significantly increase the local heat-transfer rate.

For the turbulent boundary layer Von Kármán's extension of the Reynolds Analogy is quoted (Eckert [14]):

$$\frac{Nu_x}{Re_x\,Pr} = \frac{1}{Z^2}\left\{\frac{1}{1 + (1/Z)[5(Pr - 1) + 5\log_e(5Pr + 1)/6]}\right\} \qquad (4.22)$$

in which

$$Z^2 = \rho U_x^2/\tau_{0,x}. \qquad (4.23)$$

This is related conveniently to the ordinates $Nu/Re_2^{\frac{1}{2}}$ by:

$$\frac{Nu}{Re_2^{\frac{1}{2}}} = \frac{Re_2^{\frac{1}{2}}\,U_x/U_{2c}}{(Z^2/Pr)\{1 + (1/Z)[5(Pr - 1) + 5\log_e(5Pr + 1)/6]\}} \qquad (4.24)$$

Initial thickness of the turbulent boundary layer

The calculation of the turbulent boundary layer requires knowledge of the initial turbulent momentum thickness after a laminar separation. An empirical rule is used, involving one constant, which is supported by experimental evidence.

Assuming that the volume of fluid at separation remains constant throughout separation in view of the negligible influence of skin friction, then

$$U\delta\int_0^1 (u/U)\,\mathrm{d}(y/\delta) = \text{constant} \qquad (4.25)$$

If we knew velocity profiles in the form

$$u/U = f(y/\delta)$$

for the laminar layer just before separation and for the turbulent layer just after reattachment, the ratio of the two values of δ could be computed from equation (4.25). In the absence of the requisite data, a rough calculation is made using approximate velocity profiles for the simple

case of a flat plate in zero pressure gradient, namely

$$u/U = \tfrac{3}{2}(y/\delta) - \tfrac{1}{2}(y/\delta)^3$$

for the laminar layer and

$$u/U = (y/\delta)^{\frac{1}{7}}$$

for the turbulent layer. This gives the initial value of the Reynolds number for the turbulent layer, based on momentum thickness as

$$(U\theta_x/\nu)_T = 0{\cdot}523\,(\theta_x/c)_L\,(U_L/U_T) \times (U_T/U_{2c})\,Re_2 \quad (4.26)$$

where L refers to conditions at the end of the laminar layer and T to the initial condition of the turbulent layer, U is the local velocity, and U_{2c} downstream velocity at midspan. A check of the constant in equation (4.26) is given by basing the left-hand term on values devised from known measurements of $Nu/Re_2^{\frac{1}{2}}$. This involves working in reverse order the steps relating θ_x to $Nu/Re_2^{\frac{1}{2}}$ of the preceding section. Using data for the laminar separation point at $x/c \approx 0{\cdot}7$ on the convex surface, the mean value of the constant for six streamlines taken over the complete span was found to be 0·466. This value was used in lieu of 0·523 in equation (4.26).

The position of laminar separation is determined by experiment (see [1]) and the positions consequently assumed for calculations are indicated in Figs. 6 and 7.

Further research would be necessary before any confident theoretical prediction of the transition points could be made where the influence of cross-flows is involved. Close to the end wall, there is strong interaction between boundary layer on the convex surface and the layer of the end wall of the cascade, leading to early transition.

Comparison of measured and computed heat-transfer results

To facilitate comparison with experimental data, which were obtained in planes of (x, y), it is necessary to interpolate the results of calculations (made in natural streamline co-ordinates) to these planes. Figures 6 and 7, which show experimentally determined streamline trajectories close to the boundary layers of the blade surfaces, show how interpolation may suitably be effected.

If experimental data were not available, an estimate could be made from computed values of w, provided that the transition line could be determined or assumed with confidence.

Comparisons are shown in Figs. 8–11, for the condition of zero blade incidence and $Re_2 = 3{\cdot}38 \times 10^5$.

Laminar flow regions

Convex surface. There is generally good agreement between calculations and experimental results at the stagnation point and over the fore part of the blade up to $x/c \approx 0{\cdot}75$, the results based on the first approximation θ_{I} lying generally somewhat closer to the measured values than those based on θ_{II}. Over the majority of the span, the second approximation leads to higher values of calculated heat transfer than does the first, but this situation is reversed at the station $z = 4{\cdot}5$ in near to the end of the blade.

Concave surface. In the two-dimensional mainstream zone near the midspan, conditions are predicted well up to $x/c \approx 0{\cdot}4$, where a surface roughness destabilizes the boundary layer, as discussed in reference [1]. The calculated laminar curve falls smoothly to a value of 0·32 at the trailing edge. In the region where the upstream total pressure varies, transition occurs very much earlier, namely at $x/c \approx 0{\cdot}1$, but over the short length where comparison is possible laminar heat transfer again agrees well with measurement.

Turbulent flow regions

Convex surface. The momentum thickness is chosen to be consistent with measured heat-transfer data at reattachment in the pressure rise downstream of the throat ($x/c \approx 0{\cdot}9$) according to the empirical rule of equation (4.26), using a constant of 0·466. The second

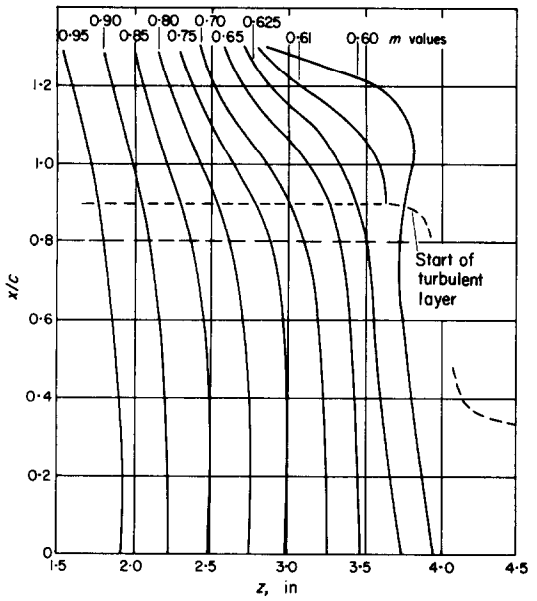

FIG. 6. Streamline configuration close to the boundary layer on convex surface.

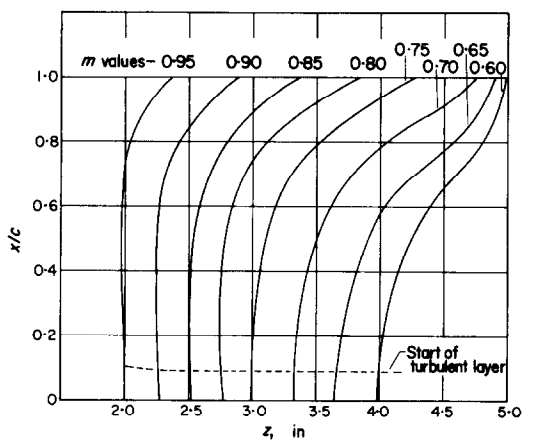

FIG. 7. Streamline configuration close to the boundary layer on concave surface.

approximation θ_{II} for momentum thickness now leads to closer agreement with experiment. At span station $z = 4{\cdot}5$ in, where there is interference between the wall and blade boundary layers, transition is assumed at $x/c = 0{\cdot}35$, turbulent separation is taken at $x/c = 0{\cdot}8$, and this is followed at $x/c = 0{\cdot}85$ by turbulent reattachment.

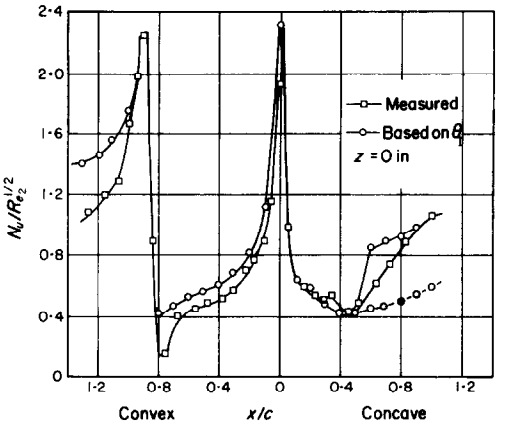

FIG. 8. Computed and measured heat-transfer coefficients at midspan.

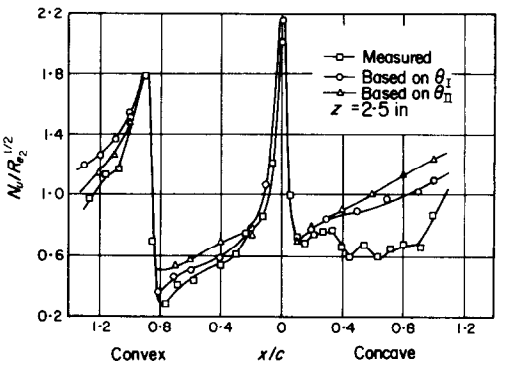

FIG. 9. Computed and measured heat-transfer coefficients at $z = 2{\cdot}5$ in.

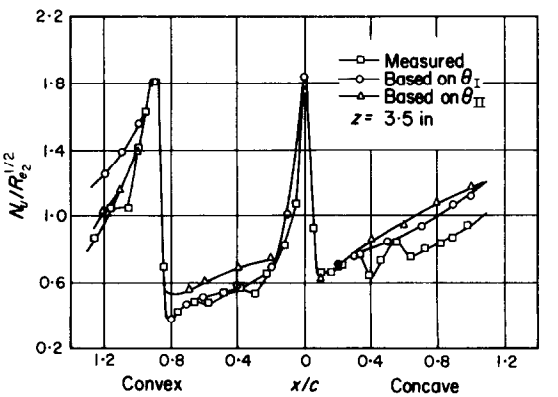

FIG. 10. Computed and measured heat-transfer coefficients at $z = 3{\cdot}5$ in.

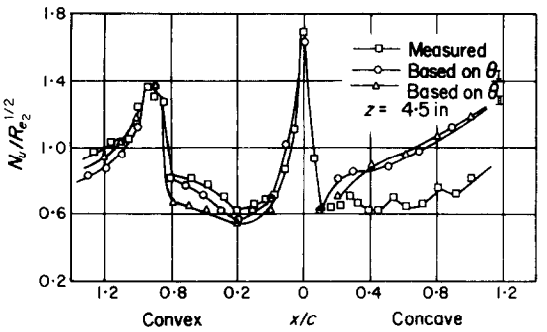

FIG. 11. Computed and measured heat-transfer coefficients at $z = 4{\cdot}5$ in.

Concave surface. The rising curve downstream of the point $x/c = 0{\cdot}4$ in the region of uniform mainstream is not anticipated by the calculations. However, two calculated curves are shown. The lower one is computed using an initial boundary-layer thickness at $x/c = 0{\cdot}4$ chosen to fit the measured heat transfer at that point. The upper curve is for a turbulent layer which is assumed to originate at the stagnation point. The experimental results are seen to lie on a line which passes from the lower to the upper calculated curve between $x/c = 0{\cdot}4$ and the trailing edge of the blade. In view of the reasonable success with calculations elsewhere on the blade, it seems that this layer is intermittently turbulent or in a state of progressive breakdown, as described previously [1].

In the region of varying total pressure, the experimental values show slowly rising curves exhibiting a more erratic behaviour than elsewhere on the surface, and which lie almost entirely below the calculated values. The skin friction according to the second approximation is generally a little greater than the first.

It will be seen that over most of the blade there is quite good agreement between computed and measured values. The influence of cross-flow on local heat transfer over the laminar flow part of the convex surface is not large, and the calculations follow this particular experimental trend extremely well. It is concluded that the methods described may be used with reasonable confidence if information on the position of the transition lines is available. Although, in the investigation of the relative accuracy of methods of various degrees of refinement, appeal has been made to experimental data in the preceding sections, it should be emphasised that in no case has the result of computation been significantly improved by incorporation of such data.

REFERENCES

1. L. A. WALKER and E. MARKLAND, Heat transfer to turbine blading in the presence of secondary flow, *Int. J. Heat Mass Transfer* **8**, 729 (1965).
2. W. R. HAWTHORNE, Rotational flow through cascades. Pt. I: The components of vorticity, *Q. Jl. Mech. Appl. Math.* **8**, 266 (1955).
3. A. MAGER, Generalization of boundary layer momentum-integral equations to three-dimensional flows including those of a rotating system, NACA Report No. 1067 (1952).
4. H. B. SQUIRE, Heat transfer calculations for aerofoils, Aero. Res. Coun. R. and M. No. 1986 (1942).
5. W. R. HAWTHORNE and W. D. ARMSTRONG, Rotational flow through cascades, Pt. II. The circulation about the cascade. *Q. Jl. Mech. Appl. Math.* **8**, 280 (1955).
6. H. B. SQUIRE and K. G. WINTER, The secondary flow in a cascade of aerofoils in a non-uniform stream, *J. Aeronaut. Sci.* **18**, 271 (1951).
7. J. H. PRESTON, A simple approach to the theory of secondary flow, *Aeronaut. Q.* **5**, 218 (1954).
8. W. R. HAWTHORNE, Secondary circulation in fluid flow, *Proc. R. Soc.* **206A**, 374 (1951).
9. W. R. HAWTHORNE and W. D. ARMSTRONG, Shear flow through a cascade, *Aeronaut. Q.* **7**, 247 (1956).
10. J. M. WILD, The boundary layer of yawed infinite wings. *J. Aeronaut. Sci.* **16**, 41 (1949).
11. R. TIMMAN, The theory of three-dimensional boundary layers. N. P. L. Symp. on Boundary Layer Effects (March, 1955).
12. L. PRANDTL, On boundary layers in three-dimensional flow. Reps. and Trans. No. 64, Min. Aircraft Prodn, G.B. (1946).
13. E. GRUSCHWITZ, Turbulent Reibungsschichten mit Sekündarströmung, *Ing.-Arch.* **VI**, 355 (1935).
14. E. R. G. ECKERT, *Introduction to the Transfer of Heat and Mass*, p. 124. McGraw-Hill, New York (1950).
15. D. J. K. STUART, Analysis of Reynolds number effects in fluid flow through two-dimensional cascades, Aero. Res. Coun. R. and M. No. 2920 (1955).

APPENDIX 1

Note on Estimation of Primary Field

The simplest model of the primary field is obtained by taking the two-dimensional potential solution of Fig. 1 and scaling all velocities

in a given (xy) plane in proportion to the known velocity at inlet. The local velocity U_{xz} at any chosen point in the blade passage at a specified spanwise station z is thus given in terms of the upstream velocity U_{1z} by

$$U_{xz}/U_{1z} = U_{xp}/U_{1p} \qquad \text{(A1.1)}$$

where the suffix p indicates the two-dimensional potential solution. Use of this simple relation leads to an overestimation of the pressure drop through the cascade, although the secondary stream deduced from it is in fair agreement with experiment.

A more realistic model is one which takes account of lateral deflection, which may be estimated from measurements within the blade passages as indicated below. It is convenient to deal with the region over which the inlet velocity profile is nearly uniform (i.e. $z < 2$ in) separately from that where the total pressure is varying rapidly (i.e. 5 in $> z >$ 2 in).

Over the region of near-uniformity, an adaptation is made of the method evolved by Stuart [15] for dealing with an apparent flow contraction in a compressor cascade. The reduction of pressure ratio across the cascade, as compared with the two-dimensional case, leads to a spanwise diffusion of the stream. Suppose that the upstream velocity U_{1z} in the flow under consideration is related to the upstream velocity U_{1p} in a corresponding two-dimensional flow by

$$U_{1z}/U_{1p} = \lambda \qquad \text{(A1.2)}$$

in which $\lambda > 1$; the velocities U_{2z} and U_{2p} downstream of the blades are equal in the two motions. We now assume that there is a relationship at the form

$$\frac{U_{xz}}{U_{xp}} = \frac{\lambda}{1 - (1 - \lambda)\chi^s} \qquad \text{(A1.3)}$$

between the velocity U_{xz} at any point of the flow and the velocity U_{xp} at the same point of the two-dimensional flow. The parameter χ varies from zero to unity through the blade passage, and s is a constant. The procedure used to determine χ may be seen by reference to Fig. 1 where the line LL' denotes the plane of the leading edges, and SS' a plane at which two-dimensional flow is substantially uniform downstream of the blades. For each streamline of the two-dimensional flow, χ is the distance from the intersection of the streamline with LL', projected in the direction of the chord, and expressed as a fraction of the projected length of the segment of the streamline contained between LL' and SS'.

The change in velocity ratio due to diffusion may then conveniently be expressed in the form

$$\frac{U_{xz}}{U_{1z}} = \frac{U_{xp}/U_{1p}}{1 - (1 - \lambda)\chi^s} \qquad \text{(A1.4)}$$

from which λ may be found by putting $\chi = 1$ and comparing the overall velocity ratio as measured in the two-dimensional flow condition with that measured in the presence of secondary flow. The exponent s is chosen to suit measured values of surface pressures along the blade chord. Writing

$$C_p = 1 - (U_{xz}/U_{2z})^2 \qquad \text{(A1.5)}$$

as the pressure coefficient and

$$C_p' = 1 - (U_{xp}/U_{2p})^2 \qquad \text{(A1.6)}$$

as the pressure coefficient for two-dimensional flow, and substituting in equation (A1.4) leads to the result

$$\left(\frac{1 - C_p'}{1 - C_p}\right)^{\frac{1}{2}} = \{1 - (1 - \lambda)\chi^s\}/\lambda \qquad \text{(A1.7)}$$

which may be rewritten to give s explicitly as

$$s = \log\{1 - \lambda[(1 - C_p')/(1 - C_p)]^{\frac{1}{2}}/(1 - \lambda)\}/\log\chi \qquad \text{(A1.8)}$$

Experimental values of C_p show that s is very nearly constant over the blade chord, indicating that the form of equation (A1.2) gives a good representation of the effect being considered. In the particular condition of the present test, λ has the value 1·24 and s is 2·7.

Over the part of the span where the total pressure is changing rapidly (5 in $> z >$ 2 in)

the above treatment requires modification to allow for changing total pressure. Using equation (A1.7) as a basis, various forms of relationship were considered to obtain an empirical matching of measured pressures calculated under two-dimensional conditions. The form adopted is

$$(1 - C_p)/(1 - C'_p) = 1 + (p\chi + q)(1 - \chi)^r \quad \text{(A1.9)}$$

in which p, q and r are constant along a blade surface at a given value of z. For flow within the blade passage, linear interpolation between the values of the constant on the concave and convex blade surfaces is adopted, values being chosen appropriate to the particular value of z. Typical values of the constants p, q and r for the particular non-uniform flow under consideration are (at $z = 3{\cdot}5$ in.) 1·00, 0·40 and 0·37 on the concave surface and 1·60, 0·20 and 1·34 on the convex surface.

The relationship which corresponds with equation (A1.4) may readily be shown to be

$$\frac{U_{xz}}{U_{1z}} = \frac{U_{xp}}{U_{2p}} \left\{ \left(\frac{mP_{2c} - p_2}{mP_{2c} - p_1} \right) \times \left(\frac{1 - C_p}{1 - C'_p} \right) \right\}^{\frac{1}{2}} \quad \text{(A1.10)}$$

where, on the blade surface, mP_{2c} is the local total pressure involved in the calculation of C_p, and in the blade passage, mP_{2c} is again the local total pressure at the point where U_{xz} is required.

APPENDIX 2

Outline of Boundary-layer Calculation

Following the analysis of Mager [3] and making slight adjustments to allow for the facts that the blades are not rotating and that the main stream is not irrotational, having a component η of vorticity just outside the boundary layer in the y direction, the momentum integral equations are

$$\frac{\partial \theta_x}{\partial \mathbf{x}} + \frac{1}{U}\frac{\partial U}{\partial \mathbf{x}}(2\theta_x + \delta_x^*) + \frac{\partial \theta_{xz}}{\partial \mathbf{z}} + \frac{2\eta}{U}\theta_{xz} = \frac{\tau_{0.x}}{\rho U^2} \quad (4.3)$$

$$\frac{\partial \theta_z}{\partial \mathbf{z}} + \frac{\partial}{\partial \mathbf{x}}(\delta_z^* - \theta_{xz}) + \frac{1}{U}\frac{\partial U}{\partial \mathbf{z}}(\theta_z - \theta_x - \delta_x^*) + \frac{2}{U}\frac{\partial U}{\partial \mathbf{x}}(\delta_z^* - \theta_{xz}) + \frac{\eta}{U}(\theta_x + \theta_z) = -\frac{\tau_{0.z}}{\rho U^2}. \quad (4.4)$$

Substitution of H, J, K, L from equations (4.9) and $\tau_{0.x}/\rho U^2$ from equation (4.15) and for $\tau_{0.z}/\tau_{0.x}$ from equation (4.8) gives, after reduction,

$$\frac{1}{n+1}\frac{\partial \boldsymbol{\theta}}{\partial \mathbf{x}} + \frac{1}{n+1}J\varepsilon\frac{\partial \boldsymbol{\theta}}{\partial \mathbf{z}} + J\boldsymbol{\theta}\frac{\partial \varepsilon}{\partial \mathbf{z}} + \boldsymbol{\theta}\left\{\frac{1}{U}\frac{\partial U}{\partial \mathbf{x}}\left[(2 + H) - \frac{n}{n+1}\right] + \frac{n}{n+1}J\varepsilon C + \frac{n+2}{n+1}\frac{J\varepsilon}{U}\eta\right\} - a = 0 \quad \text{(A2.1)}$$

$$\frac{(K - J)}{n+1}\varepsilon\frac{\partial \boldsymbol{\theta}}{\partial \mathbf{x}} + \frac{L\varepsilon^2}{n+1}\frac{\partial \boldsymbol{\theta}}{\partial \mathbf{z}} + (K - J)\boldsymbol{\theta}\frac{\partial \varepsilon}{\partial \mathbf{x}} + 2L\boldsymbol{\theta}\varepsilon\frac{\partial \varepsilon}{\partial \mathbf{z}} + \boldsymbol{\theta}\left\{\frac{n+2}{n+1}(K - J)\frac{\varepsilon}{U}\frac{\partial U}{\partial \mathbf{z}} - C\left[\frac{L\varepsilon^2}{n+1} - 1 - H\right] + \frac{\eta}{U}\left[\frac{n+2}{n+1}L\varepsilon^2 - H\right]\right\} + \varepsilon a = 0 \quad \text{(A2.2)}$$

in which

$$\boldsymbol{\theta} = \theta_x Re_\theta^n \quad (4.16)$$

and the constants a and n are available from the initial condition. Making the same assumptions as

Mager, that ε is small compared with unity, and θ is small compared with length measured along the flow path, then terms in ε^2, $\varepsilon\theta$ and θ^2 may be neglected and equations (A2.1) and (A2.2) simplify to

$$\frac{\partial\theta}{\partial \mathbf{x}} + [(n+1)(H+2) - n]\frac{1}{U}\frac{\partial U}{\partial \mathbf{x}}\theta = (n+1)a \tag{A2.3}$$

$$\frac{\partial\varepsilon}{\partial \mathbf{x}} + \left[\frac{1}{n+1}\frac{1}{\theta}\frac{\partial\theta}{\partial \mathbf{x}} + \frac{n+2}{n+1}\frac{1}{U}\frac{\partial U}{\partial \mathbf{x}} + \frac{a}{\theta(K-J)}\right]\varepsilon = \frac{1}{J-K}\left[(1+H)C - \eta\frac{H}{U}\right]. \tag{A2.4}$$

The solutions, extended to a desired value $\mathbf{x}$ from an initial value $\mathbf{x}_i$, of these equations, are obtained as follows

$$\theta_{\mathrm{I}} = \theta_i(U_i/U)^{(n+1)(H+2)-n} + \frac{(n+1)a}{U^{(n+1)(H+2)-n}}\int_{\mathbf{x}_i}^{\mathbf{x}} U^{(n+1)(H+2)-n}\,\mathrm{d}\mathbf{x} \tag{A2.5}$$

where θ_{I} is the first approximation. Using this to obtain a first approximation ε_{I} of equation (A2.4)

$$\varepsilon_{\mathrm{I}} = (\theta_i/\theta_{\mathrm{I}})^{1/(n+1)}(U_i/U)^{(n+2)/(n+1)}\frac{\varepsilon_i}{E_1(\mathbf{x})} + \frac{\int_{\mathbf{x}_i}^{\mathbf{x}} \alpha\theta_{\mathrm{I}}^{1/(n+1)}\,U^{(n+2)/(n+1)}\,E_1(\mathbf{x})\,\mathrm{d}\mathbf{x}}{(J-K)\,\theta_{\mathrm{I}}^{1/(n+1)}\,U^{(n+2)/(n+1)}\,E_1(\mathbf{x})} \tag{A2.6}$$

in which

$$E_1(\mathbf{x}) = \exp\left(\frac{a}{K-J}\int_{\mathbf{x}_i}^{\mathbf{x}}\frac{\mathrm{d}\mathbf{x}}{\theta}\right) \tag{A2.7}$$

and

$$\alpha = (H+1)C - H\eta/U. \tag{A2.8}$$

The terms involving ε in equation (A2.1) may now be taken into account. The reduced form, equation (A2.3) becomes:

$$\frac{\partial\theta}{\partial \mathbf{x}} + J\varepsilon\frac{\partial\theta}{\partial \mathbf{z}} + \theta\left\{\frac{1}{U}\frac{\partial U}{\partial \mathbf{x}}[(n+1)(H+2) - n] + n\varepsilon JC + (n+2)\frac{J\varepsilon}{U}\eta\right\} = (n+1)a \tag{A2.9}$$

admitting a small loss of accuracy in the neglect of the term $J\theta\,\mathrm{d}\varepsilon/\mathrm{d}\mathbf{z}$. Mager suggests the use of Lagrange's method to obtain the improved value, say θ_{II}, from this equation. However, if $\partial\theta_{\mathrm{I}}/\partial\mathbf{z}$ and $\partial\theta_{\mathrm{II}}/\partial\mathbf{z}$ are taken to be equal, the solution is:

$$\theta_{\mathrm{II}} = (U_i/U)^{(n+1)(H+2)-n}\frac{\theta_i}{E_2(\mathbf{x})} + \frac{\int_{\mathbf{x}_i}^{\mathbf{x}} U^{(n+1)(H+2)-n}\,E_2(\mathbf{x})\{(n+1)a - J\varepsilon\,\partial\theta_{\mathrm{I}}/\partial\mathbf{z}\}\,\mathrm{d}\mathbf{x}}{U^{(n+1)(H+2)-n}\,E_2(\mathbf{x})} \tag{A2.10}$$

in which a and n are known, and $E_2(\mathbf{x})$ is

$$E_2(\mathbf{x}) = \exp\left\{\int_{\mathbf{x}_i}^{\mathbf{x}} J\varepsilon[nC + (n+2)\eta/U]\,\mathrm{d}\mathbf{x}\right\}. \tag{A2.11}$$

Clearly the accuracy of the calculation, which starts from a two-dimensional approximation and proceeds to correct this for cross-flow effects, depends on the accuracy with which the two-dimensional value of momentum thickness is first predicted.

Résumé—Dans un article précédent [1], l'on a décrit des mesures de coefficients locaux de transport de chaleur sur la surface d'une ailette de turbine à gaz dans une grille d'aubes où se produit un écoulement secondaire important. On donne maintenant les détails des calculs, en les considérant en deux parties, (a) l'estimation des vitesses d'écoulement secondaire et (b) la nature de la couche limite sur l'ailette et les propriétés du transport de chaleur qui y sont liées.

Dans la première partie, les calculs pour la vorticité longitudinale induite sont basés sur la méthode de Hawthorne [2]. Les calculs sont effectués grâce à trois hypothèses sur l'écoulement principal, avec plusieurs degrés de complexité. Dans le cas le plus simple, on suppose que l'on a un écoulement de tourbillon libre, dans le cas suivant, on utilise un champ connu de vitesses bidimensionnelles autour des ailettes, et enfin, on le corrige pour tenir compte du déplacement de l'écoulement principal.

Les résultats ne diffèrent pas beaucoup l'un de l'autre, et l'accord avec l'expérience est généralement bon. Les calculs de couche limite emploient les relations intégrales de quantité de mouvement sous la forme due à Mager [3] pour l'écoulement tridimensionnel. On les a adapté pour tenir compte de la vorticité dans l'écoulement général, où cela est important, et pour y incorporer une loi de frottement pariétal delus générale.

Le transport de chaleur dans la couche laminaire est calculé par la méthode de Squire [4], et pour la couche limite turbulente en utilisant l'extension de Von Karman de l'analogie de Reynolds. La difficulté de prévoir les conditions après un décollement laminaire a rendu nécessaire d'établir les données initiales, dans le cas d'une couche turbulente qui se recolle, sur une loi empirique obtenue à partir des résultats expérimentaux de transport de chaleur et que l'on suggère d'appliquer plus largement.

La comparaison avec l'expérience est bonne lorsque la couche limite est laminaire, mais le transport de chaleur est surestimé dans les régions turbulentes, particulièrement en présence d'un gradient de pression favorable.

Zusammenfassung—Eine frühere Arbeit [1] befasste sich mit Messungen der örtlichen Wärmeübergangskoeffizienten an Gasturbinen in Kaskadenanordnung, wobei eine starke Zweitströmung erzeugt wurde. Einzelheiten der Berechnung werden nun gebracht; die Arbeit wird als zweiteilig angesehen: (a) die Bestimmung der Zweitstromgeschwindigkeiten und (b) die Natur der Schaufelgrenzschicht und einschlägige Stoffwerte für den Wärmeübergang.

Die Berechnungen im ersten Teil für die aufgebrachte Verwirbelung in Strömungsrichtung beruhen auf einer Methode von Hawthorne [2]. Die Berechnungen wurden durchgeführt mit drei Annahmen unterschiedlicher Feinheit für den Hauptstrom. Die Ergebnisse unterscheiden sich nicht stark voneinander und die Übereinstimmung mit dem Versuch ist im Allgemeinen gut.

In den Grenzschichtberechnungen werden die Momentenintegralbeziehungen in der Form nach Mager [3] für die dreidimensionale Strömung benützt. Angleichungen werden vorgenommen, um die Verwirbelung im Hauptstrom zu berücksichtigen, soweit dies notwendig ist, und um ein allgemeineres Gesetz für die Oberflächenribung einzuführen.

Der Wärmeübergang in der Laminarschicht wird nach der Methode von Squire [4] berechnet, für die turbulente Grenzschicht nach der Erweiterung der Reynolds Analogie durch von Kármán. Die Schwierigkeit, Bedingungen vorherzubestimmen, die einer laminaren Ablösung folgen machte es notwendig, die Anfangswerte für das Wiederanlegen der turbulenten Schicht auf eine empirische Regel zu beziehen, die, gewonnen aus gemessenen Wärmeübergangswerten, versuchsweise zu weiterer Anwendung vorgeschlagen wird.

Der Vergleich mit dem Versuch liefert gute Übereinstimmung bei laminarer Grenzschicht; in den turbulenten Bereichen wird aber der Wärmeübergang überschätzt, besonders, wenn ein günstiger Druckgradient vorliegt.

Аннотация—В предыдущей статье [1] описывались измерения коэффициента локального теплообмена на поверхности лопатки газовой турбины в каскаде, где создавался силный вторичный поток. В настоящей статье приводятся подробные расчеты, причем работа разбивается на две части, (а) количественное определение скорости вторичного потока и (б) природа пограничного слоя на лопатке и связанные с ним теплообменные характеристики.

В первой части расчеты вынужденной завихренности потока основаны на методе Хосорна [2]. Расчеты основного потока приводятся с тремя последовательными допущениями. Вначале предполагается свободный вихревой поток, далее используется известное двухмерное поле скоростей у лопаток и, наконец, все это корректируется для того, чтобы учесть смещение основного потока. Результаты сильно отличаются друг от друга, и, в общем, находятся в хорошем соответствии с Экспериментальными данными.

При расчете пограничного слоя используются интегральные соотношения количества движения для трехмерного потока по Мэйджеру [3]. Сделаны некоторые упрощения, чтобы учесть завихренность основного потока и получить более общий закон поверхностного трения.

Теплообмен в ламинарном слое рассчитывается по методу Сквайера [4] для турбулентного пограничного слоя с помощью аналогии Рейнольдса по Карману. Трудность расчета условий, при которых возникает отрыв ламинарного слоя, привела к необходимости брать начальные данные для присоединившегося слоя на основании эмпирического правила, которое составлено на основании данных, полученных при измерениях теплообмена, и произвольно предполагается годным для облее широкого использования.

Сравнение с экспериментальными данными показало хорошее совпадение для ламинарного пограничного слоя, а в турбулентной области значения коэффициента теплообмена получаются завышенными, особенно, при наличии отрицательного градиента давления.